JOURNAL OF MATERIALS SCIENCE 31 (1996) 1319–1325

Kinetic studies of tricalcium silicate formation from sol–gel precursors

Y. WANG, W. J. THOMSON
Department of Chemical Engineering, Washington State University, Pullman, WA 99164, USA

Reaction kinetic studies of Ca_3SiO_5 formation from sol–gel-derived precursors were carried out *in situ* using dynamic X-ray diffraction. Infrared spectra data, TEM experimental results, and X-ray diffraction patterns, all confirmed that CaO and Ca_2SiO_4 are the only compounds formed from a stoichiometric gel prior to Ca_3SiO_5 formation ($< 1250\,^{\circ}C$). The kinetic data for Ca_3SiO_5 formation are consistent with an Avrami nucleation and growth mechanism but with a sudden drop in the time exponent at higher conversion. The sharp drop of the exponent is attributed to the impingement of grain growth in the longitudinal direction and this is confirmed by SEM observations of the fully converted gels. The presence of 10% steam did not change the mechanism nor the activation energy of the reaction but significantly enhanced the nucleation and grain growth rate at both stages of the reaction.

1. Introduction

Solid-state reactions in the system CaO/SiO_2 are of great interest in cement clinker manufacturing. In order to have reliable process design and plant operations, an understanding of the reaction mechanism and kinetics for the formation of cement clinker is required. Because a large fraction of Portland cements is composed of Ca_3SiO_5 (C_3S), which is the most powerful hydraulic constituent of the cement, the formation of C_3S from Ca_2SiO_4 (C_2S) and CaO is particularly important. In fact, this reaction is known to be the slowest in the sequence of reaction steps leading to clinker manufacturing [1]. The C_2S–CaO reaction system is also the model of the last reaction stage in the formation of C_3S synthesized from CaO or $CaCO_3$ and SiO_2 with C_2S being formed at the first stage. Based on the phase diagram of the $CaO–SiO_2$ system [2], it is common opinion that C_3S is in a stable state at $> 1250\,^{\circ}C$ and is in equilibrium with C_2S and CaO at $1250\,^{\circ}C$.

The formation rate of C_3S is significantly affected by the fineness and homogeneity of the starting materials. Christensen and co-workers [3, 4], Hrabe and Jesenak [5], and Chesley and Burnet [6] studied pellets of powdered samples (in the micrometre-size range) and found that the formation of C_3S from CaO and C_2S is a diffusion-controlled reaction. The ability to synthesize C_3S at lower temperatures will result in a more economical energy consumption but will depend on the ability to combine reagents in a finer size range, so that the kinetics of formation are reasonably fast. One example of such an approach is the use of sol–gel methods to synthesize C_3S as reported by Li and Roy [7]. The application of sol–gel methods allows for the possibility of mixing the reagents in a finer range and thus manufacturing the cement at relatively low temperatures and in a shorter time. Under these conditions, the diffusion path lengths should be minimized and the C_3S formation kinetics may not be a diffusion-controlled process. Even though Li and Roy [7] used a sol–gel method to synthesize C_3S, they did not attempt to quantify the reaction kinetics of C_3S formation from their sol–gel precursors. Consequently, we report here a study of the transformation kinetics of C_3S from a mixture of C_2S and CaO prepared by a sol–gel method, where the kinetics were followed with dynamic X-ray diffraction (DXRD). In addition to DXRD measurements, the chemical compositions and structures of the gel and the final products were also characterized by Fourier transform–infrared spectroscopy (FT–IR) and transmission and scanning electron microscopy (TEM and SEM). Complementary kinetic measurements were also conducted by observing thermal effects of the reactions occurring over the temperature range of interest using differential thermal analysis (DTA).

In addition to the fineness and homogeneity of the precursors, the presence of a liquid phase or different gaseous environments during high-temperature processing can also influence the reaction kinetics. For example, Christensen *et al.* [8] and Jawed *et al.* [9] both reported that the ion-rich melt phases promote the consumption of lime and thus, C_3S formation rates. It is well known that the solid-state reaction rate can be influenced by the gaseous environments even in systems where the components do not alter their oxidation state and/or in which thermal decomposition does not take place. Jesenak and Hrabe [10, 11] found that reactions between CaO and SiO_2 were enhanced by lowering the oxygen or CO_2 partial pressures but

0022–2461

were not affected by hydrogen. Although the accelerating effect of water vapour on the reaction rate in the $CaO–SiO_2$ system has been observed [10–14], there is little agreement on the cause. Montierth *et al.* [12] proposed the formation of a metastable solid solution of calcium in quartz promoted by the presence of water vapour. Jesenak and Hrabe [10] attributed the effect to hydration of the product layer through which diffusion is enhanced. Burte and Nicholson [13] ascribed the effect of steam to an increase of diffusion sites for the calcium ion in the product layer. On the other hand, Kridelbaugh [14] concluded that the presence of steam promoted the formation of monosilic acid which acts as the carrier to silicon in the fluid phase, so that SiO_2 becomes the mobile species. Because the aforementioned studies were all based on powdered samples in the micrometre-size range where the reaction rate was controlled by a diffusion mechanism, the accelerating effect of steam was reasonably attributed to the enhancement of the diffusion rate. For the small particle sizes associated with sol–gel precursors, diffusion should be less of a factor and water vapour could play a different role in affecting the formation rate of C_3S. Therefore, another goal of this study was to investigate the influence of the water vapour on the formation kinetics of C_3S from C_2S and CaO mixtures synthesized by the sol–gel method.

2. Experimental procedure

A gel with a stoichiometric tricalcium silicate composition (Ca/Si = 3/1) was prepared by the same method as described by Li and Roy [7]. $Ca(NO_3)_2$ was first prepared by mixing $CaCO_3$ (Mallingkrodt Chemical Works) with a suitable quantity of HNO_3, diluted with deionized water, and then mixed with a diluted Ludox sol (AS grade, E.I. duPont de Nemours company). The above solution was heated at 70 °C and agitated with a magnetic stirrer on a hot plate until gelation was observed to occur (about 6 h). The gel was then dried overnight in an oven at 90 °C.

Some of the dried gel materials were heated from room temperature to 1400 °C in order to follow the complete phase development from the precursors; others were pre-heated at ~ 760 °C in an atmospheric oven for 1 h to decompose $Ca(NO_3)_2$ and to synthesize the C_2S–CaO mixture which was used to study the kinetics of C_3S formation. Kinetic measurements were performed *in situ* with DXRD which consists of a Siemens D500 diffractometer (CoK_α radiation) equipped with a position sensitive detector and an Anton-Paar hot stage. This technique allows for the *in situ* monitoring of solid-state transformations as fast as every 5 s. Details of the technique have been previously described by Thomson [15]. Both isothermal ($\pm$ 1 °C) and non-isothermal (5 °C min^{-1}) experiments were carried out in this study. Because the DXRD measurements were conducted *in situ*, no internal standard was needed here. The extent of C_3S formation was measured by following the disappearance of CaO in the sample mixture, which was calculated by subtracting the ratio of the integrated intensities of the 200 peak of CaO to its initial integrated intensity from one.

In order to conduct kinetic measurements in a steam environment, a syringe pump (model 341B, Orion Research Inc.) was used to steadily inject deionized water at specific flow rates into flowing air which was heated above 100 °C to achieve various H_2O partial pressures. The gas inlet and chamber wall of the hot stage were also heated to about 90 °C to avoid steam condensation. For the purpose of providing a comparison with the DXRD results, DTA measurements were also carried out in a Perkin–Elmer DTA 1700 differential thermal analyser at a heating rate of 5 °C min^{-1}. Some samples were also heat treated in an oven for 1 h at various temperatures from 400–1600 °C and then analysed by TEM (Hitachi H600 with a Kevex 7000 energy dispersive X-ray spectroscopy), SEM (Hitachi S570 with an ETEC Autoscan), and transmission FT–IR (Bruker IR/98 vacuum optical bench with a MCT detector).

3. Results and discussion

3.1. Structural development of the gel

Fig. 1 shows typical DXRD results for the crystalline structural evolution of the gel heated from 360–1410 °C at 5 °C min^{-1}. At < 600 °C, $Ca(NO_3)_2$ is the only crystal phase that could be identified. $Ca(NO_3)_2$ decomposes to CaO at ~600 °C, and some of the newly formed CaO immediately reacts with SiO_2 to form monoclinic β-C_2S. The disappearance of the 3 0 1 peak of β-C_2S at ~40 °C 2θ between 650 and 1000 °C is due the phase transformation from monoclinic β-C_2S to rhombohedral α′-C_2S (there are no separate peaks for α′-C_2S). According to the phase diagram of the $CaO–SiO_2$ system [2], the rhombohedral α′-C_2S is the only stable phase between ~ 725 and 1250 °C in the $CaO–SiO_2$ system with an atomic Ca/Si ratio of 3. Finally, rhombohedral C_3S forms from CaO and α′-C_2S at about 1400 °C. A DTA scan of the gel under the same conditions is shown in Fig. 2. The endothermic peak at ~556 °C shows that

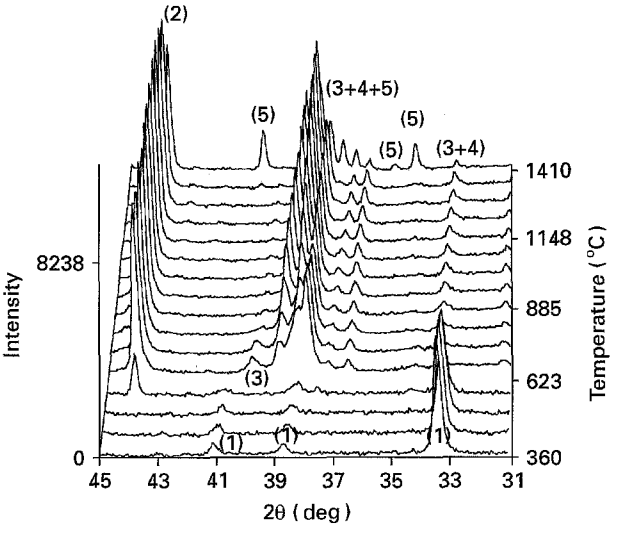

Figure 1 DXRD scan of the gel at 5 °C min^{-1} in air. (1) $Ca(NO_3)_2$ (2) CaO, (3) β-Ca_2SiO_4, (4) α′-Ca_2SiO_4, (5) Ca_3SiO_5.

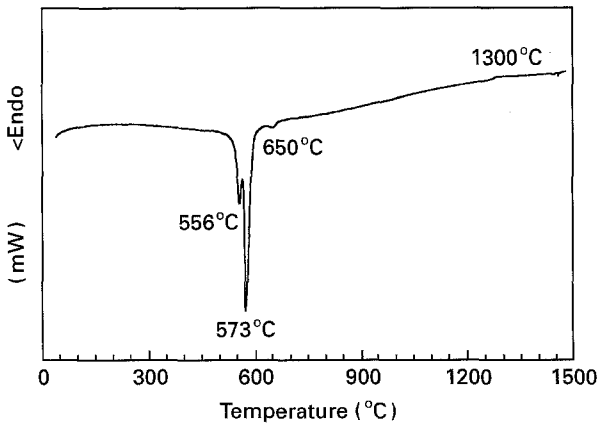

Figure 2 DTA scan of the gel at 5 °C min^{-1} in air.

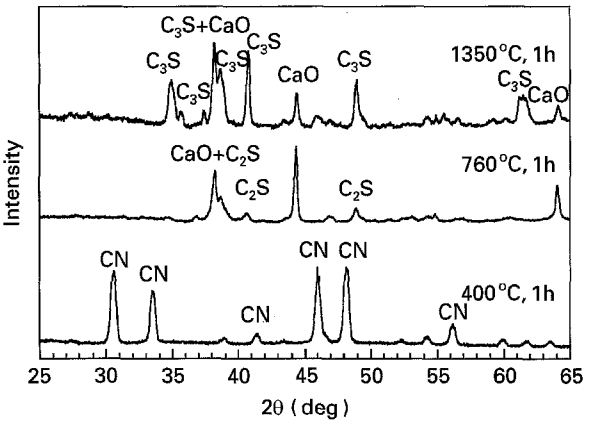

Figure 3 Powder XRD scans (gels: oven sintered and quenched to room temperature). CN, $Ca(NO_3)_2$; C_2S, Ca_2SiO_4, C_3S, Ca_3SiO_5.

$Ca(NO_3)_2$ melts first prior to decomposition, as expected. The adjacent endothermic peak at $\sim 573\,^{\circ}C$ corresponds to $Ca(NO_3)_2$ decomposition. Because the melting and decomposition of $Ca(NO_3)_2$ occurred at very close temperatures, they are not obviously distinguished in the DXRD experimental results shown in Fig. 1. The endothermic concave peak at $\sim 650\,^{\circ}C$ indicates the phase transformation of monoclinic β-C_2S to rhombohedral α'-C_2S and is consistent with the disappearance of the β-C_2S peak in the DXRD results (Fig. 1). This observation is also consistent with Coughlin and O'Brien's work [16] which showed that this phase transformation takes place at $\sim 700\,^{\circ}C$ with a small amount of endothermic reaction heat (0.440 kcal mol^{-1}). The small exothermic hump at $\sim 1300\,^{\circ}C$ is associated with the slow formation of C_3S which was also seen in the DXRD results (Fig. 1). Based on the above DXRD and DTA results, the evolutionary series of events leading from the gel to C_3S formation can be expressed as

$$3Ca(NO_3)_2(s) \rightarrow 3Ca(NO_3)_2(l) \quad \text{at} \sim 556\,^{\circ}C \quad (1)$$

$$3Ca(NO_3)_2(l) \rightarrow 3CaO + 6NO_2\uparrow + 1.5O_2 \quad \text{at} \sim 573\,^{\circ}C \quad (2)$$

$$2CaO + SiO_2\,(\text{amorphous}) \rightarrow \beta\text{-}C_2S \quad \text{at} \sim 600\,^{\circ}C \quad (3)$$

$$\beta\text{-}C_2S \rightarrow \alpha'\text{-}C_2S \quad \text{at } 650\text{–}1000\,^{\circ}C \quad (4)$$

$$\alpha'\text{-}C_2S + CaO \rightarrow C_3S \quad \text{at} > 1250\,^{\circ}C \quad (5)$$

The above results were also corroborated by FT–IR, XRD, as well as TEM analyses. Figs 3 and 4, respectively, show XRD scans and the FT–IR absorbance spectra of samples which were heat treated at three different temperatures. Only crystalline $Ca(NO_3)_2$ peaks were found in XRD patterns of the gel heated at 400 °C for 1 h, while the infrared spectra of the same sample shows not only the absorbance bands of $Ca(NO_3)_2$ (1350, 1380, 1440, and 1630 cm^{-1}) but also the characteristic bands of amorphous SiO_2 at 1100 and 780 cm^{-1} which are attributed to the Si–O stretching and bending motions. For samples heated at 760 °C for 1 h, these absorbance bands disappeared and the Ca–O–Si bands between 800 and 1100 cm^{-1} (corresponding to C_2S) and the Ca–O band at 1450 cm^{-1}, were observed (due to the decomposition of $Ca(NO_3)_2$) and the subsequent formation of C_2S). The XRD results of the sample heat treated at 760 °C

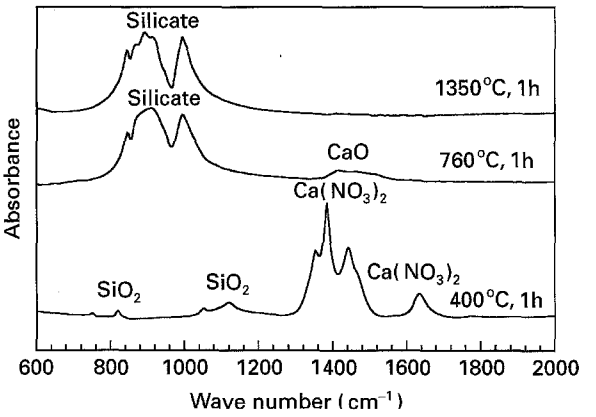

Figure 4 Infrared absorbance spectra (gels: oven sintered and quenched to room temperature).

(Fig. 3) are entirely consistent with the infrared results, i.e. the detectable crystalline phases are C_2S (in both β and α' forms) and CaO. No observable Si–O bands indicates that free SiO_2 in the sample at 760 °C is negligible. When the sample was heated at 1350 °C, three distinguishable peaks appear at ~ 850 cm^{-1} which used to have a single band at 760 °C. This may indicate the changes in the environment of Ca–O–Si vibration which resulted from the incorporation of CaO into C_2S. Again, as can be seen in Fig. 3, the XRD results are consistent with the infrared observation.

A transmission electron micrograph of the sample heat treated at 760 °C for 1 h (Fig. 5) shows clusters of very small particles in the nanometre range. Under TEM, energy dispersive X-ray spectroscopy (EDX) measurements on the same sample showed that only C_2S and CaO were observed, which is also consistent with the FT–IR results (Fig. 4). A scanning electron micrograph of a sample which was heat treated at 1600 °C for 2 h (Fig. 6), demonstrates that the grains of the final product, C_3S, have essentially equiaxed shapes with an almost perfectly smooth and clean surface. The structures of the final C_3S product were also studied with DXRD. Comparing the scans shown in Fig. 7 to the JCPDS patterns, the *in situ* XRD spectra of the C_3S product after heating at 1450 °C for 2 h reveals a rhombohedral crystalline structure (JCPDS pattern 16–406) which transfers to a triclinic structure (JCPDS pattern 31–301) when cooled to room temperature.

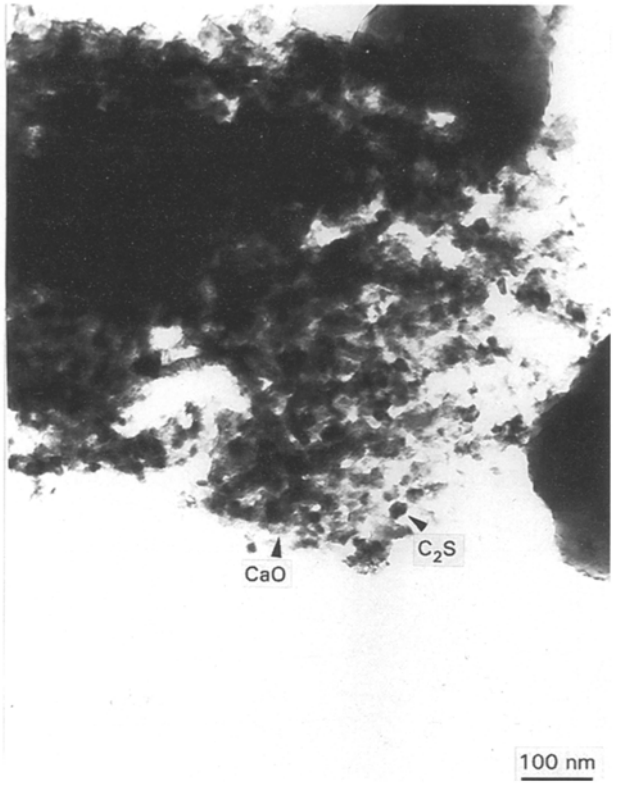

Figure 5 Transmission electron micrograph: gel heat treated at 760 °C for 1 h.

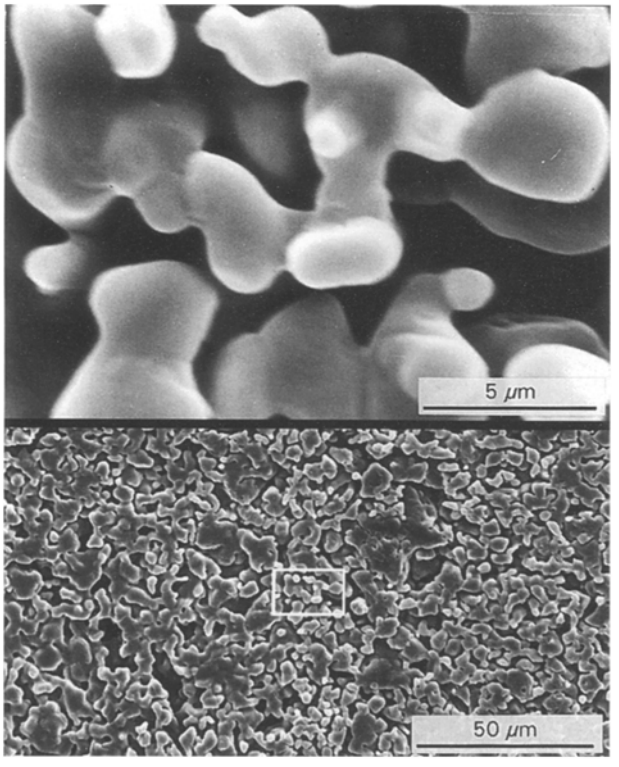

Figure 6 Scanning electron micrograph: gel heat treated at 1600 °C for 2 h.

3.2. C_3S formation kinetics

Fig. 8 shows the conversion of C_3S versus isothermal sintering time at four different temperatures in air. The data scatter, especially at high temperatures, is due to the fact that the kinetic measurements are extremely

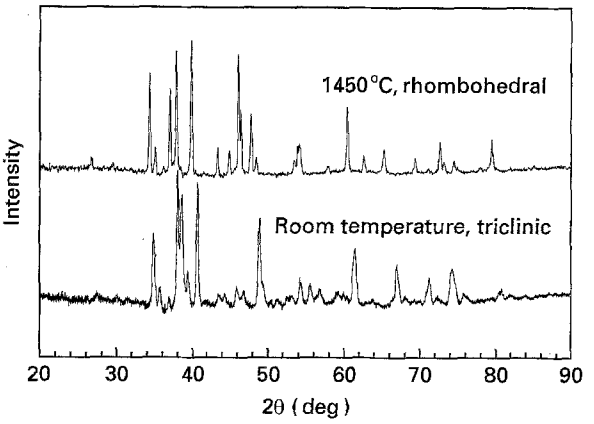

Figure 7 XRD scans of gel at 1450 °C and quenched to room temperature from 1450 °C.

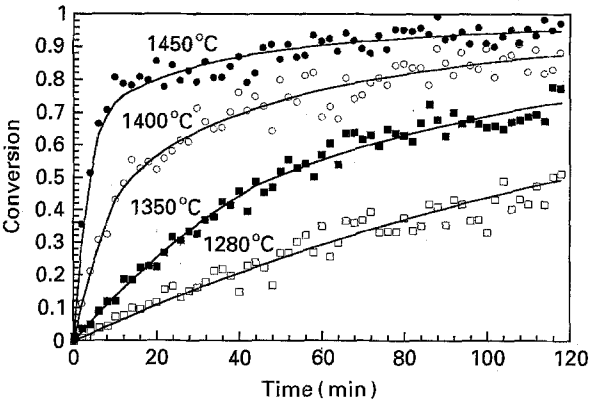

Figure 8 Conversion of Ca_3SiO_5 as a function of time and temperature in air.

sensitive to fluctuations in the X-ray source and the position-sensitive detector. However, the run-to-run experimental results demonstrate that repeatable results can be obtained within the data scatter. Basically, the reaction rate equations which are typically used for fitting solid-state reaction kinetics, can be divided into three groups: (1) diffusion-controlled reactions, (2) first-order, phase-boundary-controlled reactions, and (3) nucleation and growth-controlled reactions which obey the Avrami equation. Given that samples of C_2S and CaO prepared by sol–gel methods as used here have particle sizes in the nanometre range (Fig. 5), the diffusion path lengths are significantly reduced, and accordingly, an Avrami nucleation and growth-controlled model [17–19] might be expected. This equation can be written as

$$x = 1 - \exp(-kt^n) \quad (6)$$

or

$$\ln[-\ln(1-x)] = \ln k + n\ln t \quad (7)$$

where k is a constant which depends in part on the nucleation frequency and also on the linear rate of grain growth, and n is a constant that can vary according to the geometry of the system. The constants k and n can be determined from the intercept and slope respectively of a $\ln[-\ln(1-x)]$ versus $\ln(t)$ plot of the experimental data. Consequently, the C_3S conversion

data shown in Fig. 8 were replotted in Fig. 9 with the coordinates $\ln[-\ln(1-x)]$ versus $\ln(t)$. As can be seen from the plot, the data at 1280 °C can be fit over the entire data set ($0 < x \lesssim 50\%$) with a straight line with a slope equal to one, while the data at 1350, 1400, and 1450 °C can be approximated by two intersecting straight lines with initial slopes of one ($x' \lesssim 60\%$) and, at higher conversions, with slopes less than one. Another interesting feature is that the slopes of the straight lines at the high conversion decrease with temperature.

Several possible explanations can be found in the literature for the change of slopes. Avrami [17–19] predicted that n would decrease by one when the pre-existing nucleation sites in the transforming material were exhausted. Rollett *et al.* [20] showed that the lowering of n can be caused by variable nucleation and growth rates. However, Hancock and Sharp [21] demonstrated that the decrease of the exponent to less than one essentially represents a different reaction mechanism; specifically, a diffusion-controlled mechanism. Rosen *et al.* [22], on the other hand, explained the observed decrease of the exponent in their study of the recrystallization of iron in terms of the impingement of growing grains in the axial direction causing the grains to grow in the transverse direction.

When variable nucleation and growth rates exist, the slope of the Avrami plot should decrease gradually with time rather than the sharp transition observed here. If a diffusion-controlled mechanism was prevalent, then this diffusion-controlled mechanism should not change with temperature, i.e. the exponent should not change at different temperatures [11] as it does in Fig. 9 (0.72–0.33 at temperatures of 1350–1450 °C). Thus it appears that neither a variable nucleation rate nor a diffusion-controlled process is responsible for the observed behaviour. The sharp transition in the Avrami plot (Fig. 9) is very similar to that observed by Rosen *et al.* [22] where the slope change was attributed to the impingement of growing grains. On this basis, we also conclude that the change of the Avrami slope observed here is the result of the impingement of growing C_3S grains. The decrease of n with increasing temperature can be explained in terms of the dependence of nucleation on temperature, i.e. at higher temperatures, the rates of nucleation are higher and nucleation occurs more randomly throughout the specimen. This would lead to a more severe impingement of the faster growing C_3S grains and, thus, a more dramatic reduction in n.

Theoretical treatment [22] shows that when $0.5 \leqslant n \leqslant 1.5$, the grains grow only in one direction. Because the initial value of n is one in this study, the initial grain growth is one-dimensional. Once impingement occurs in the axial direction, the grains are free to grow only in the transverse direction. It is, therefore, not surprising that when C_3S conversion is completed, the final crystalline structure is rhombohedral as can be seen in the XRD spectra (Fig. 7). It is also noted that some of the n values are below the theoretical limit ($0.5 \leqslant n \leqslant 1.5$) for a one-dimensional mechanism (e.g. $n = 0.33$ in air at 1450 °C after the sharp transition). This discrepancy may be attributed to the fact that grain growth did not take place uniformly in all directions, as assumed for the theoretical treatment [22].

3.3. Effect of steam on the kinetics of C_3S formation

The effect of steam on reactions in the CaO (or $CaCO_3$)–SiO_2 system, where the reactions are diffusion-controlled, has been widely studied, and accelerated reaction rates due to the presence of steam have been attributed to enhanced diffusion [10–14]. However, very little is known about the effect of steam in the CaO (or $CaCO_3$)–SiO_2 systems where nucleation and growth is the controlling factor, as was the case in this study.

The formation of C_3S from a mixture of C_2S and CaO prepared by the sol–gel routine was studied at 1280, 1350, 1400, and 1450 °C, with the presence of 10% steam in air. Fig. 10 shows the data profile at 1350 °C with and without the presence of 10% steam in air. While the presence of steam did not affect the reaction sequence, it does increase the C_3S formation rate significantly. The data in Fig. 10 were also plotted in the form of $\ln[-\ln(1-x)]$ versus $\ln(t)$ and this is shown in Fig. 11. As can be seen from this plot, the data in the presence of 10% steam can also be fit with two straight lines. The initial slope of the straight line is one and then drops to less than one at ~70%

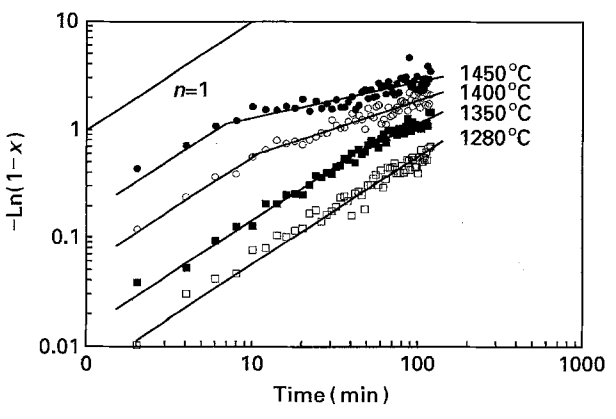

Figure 9 Avrami plots of isothermal conversions in air.

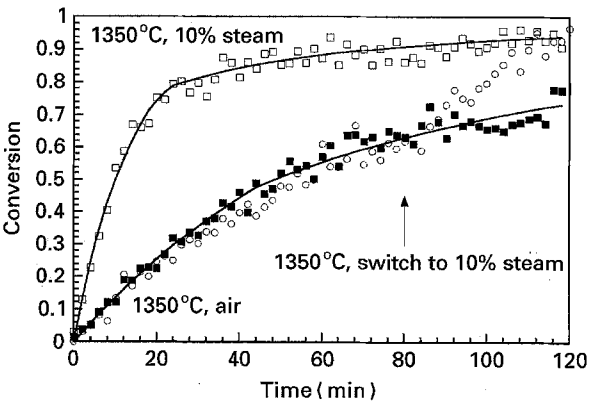

Figure 10 Conversion of Ca_3SiO_5 in both air and 10% steam at 1350 °C.

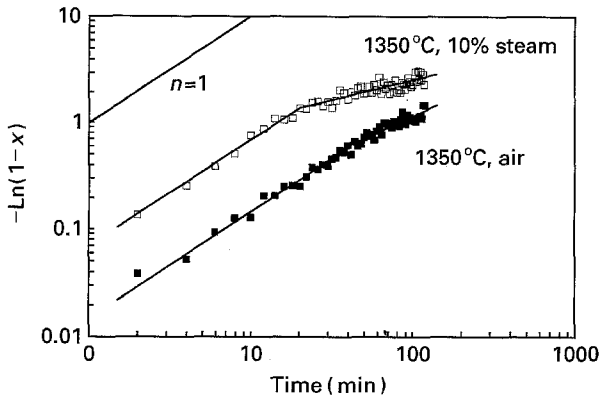

Figure 11 Avrami plots of isothermal conversions in both air and 10% steam at 1350 °C.

conversion. This same abrupt change in n was also found for the results in air except, in that case, the transition point occurred at a lower conversion (~60%). In addition, the presence of steam did not affect the activation energy at the beginning of the reaction (447.5 kJ mol^{-1} in steam versus 455.9 kJ mol^{-1} in air). Consequently, it is reasonable to conclude that the presence of steam does not affect the mechanism of C_3S formation. As stated above, the rate of nucleation and grain growth controls initial C_3S formation, but later, above the sharp transition, slower growth occurs in the transverse direction due to the impingement of grain growth in the longitudinal direction. Therefore, the effect of steam at the beginning of the reaction can probably be attributed to either the enhanced mobility of Ca^{2+} or the lowering of surface tension by the surface adsorption of H_2O which, in turn, increases the nucleation and growth rates. A similar effect of steam on the enhanced nucleation rate of mullite formation from single-phase gels has also been reported previously [23]. The fact that the transition point occurs at a higher conversion in the presence of steam can be explained in terms of the manner in which nucleation and grain growth takes place. That is, nucleation does not take place randomly over the entire sample. Some of the sample grains remain stable and they can only be consumed by the growth of neighbouring C_3S grains, which is, however, a slower process. Steam apparently stimulates these stable grains so that they also nucleate and grow in the longitudinal direction. As a result, there is a higher conversion before grain-growth impingement occurs and, in fact, the value of n is less than it is in the absence of steam (0.37 versus 0.72).

The effect of steam on C_3S formation above the sharp transition point, where the reaction is controlled by transverse grain growth, was also studied. For comparison purposes, a sample was initially heated at 1350 °C in air for 80 min so that the reaction was above the transition, at which point, an air environment containing 10% steam was introduced. These experimental results are also plotted in Fig. 10 (open circles). Within the data scatter, the results over the first 80 min are essentially the same as those in an earlier run which was conducted in air (filled squares). It is quite apparent that the introduction of 10% steam at 80 min increased the reaction rate at this stage compared to those in air. The explanation offered here is that steam initiates the longitudinal growth of those grains which had remained stable up to that point. Once steam is introduced, the conversion is then representative of some grains growing longitudinally and others growing transversely (due to grain impingement). This is also consistent with the value of n in this region, which was 0.90, a value between 1 (longitudinal growth) and 0.37 (transverse growth).

4. Conclusion

The kinetics of C_3S formation from a mixture of C_2S and CaO, synthesized by a sol–gel routine, have been studied using DXRD within the temperature range of 1280–1450 °C. The reaction kinetics were found to follow a two-stage Avrami nucleation and growth-controlled mechanism with a first stage activation energy of 455.9 kJ mol^{-1} and a value of $n = 1$. This n value is consistent with one-dimensional longitudinal growth. The existence of a two-stage reaction mechanism is attributed to the impingement of grain growth in the longitudinal direction. It was also found that the presence of steam acted to promote the reaction rate during both stages of the reaction. It is hypothesized that, after surface adsorption, steam enhances the nucleation rate of both fast and slow growing grains.

References

1. V. JOHANSEN, *J. Am. Ceram. Soc.* **56** (1973) 450.
2. B. PHILLIPS and A. MUAN, *ibid.* **42** (1959) 413.
3. N. H. CHRISTENSEN and K. A. SIMONSEN, *ibid.* **53** (1970) 361.
4. N. H. CHRISTENSEN and O. L. JEPSEN, *ibid.* **54** (1971) 208.
5. Z. HRABE and V. JESENAK, *Cem. Concr. Res.* **10** (1978) 195.
6. J. A. CHESLEY and G. BURNET, *ibid.* **19** (1989) 837.
7. S. LI and D. M. ROY, *J. Mater. Res.* **3** (1988) 380.
8. N. H. CHRISTENSEN, O. L. JEPSEN and V. JOHANSEN, *Cem. Concr. Res.* **8** (1978) 693.
9. I. JAWED, J. F. YOUNG, A. GHOS and J. SKALNY, *ibid.* **14** (1984) 99.
10. V. JESENAK and Z. HRABE, in "Proceedings of the 8th International Symposium on Reactions in Solids" (1976) p. 325.
11. Z. HRABE and V. JESENAK, *Cem. Concr. Res.* **10** (1978) 195.
12. M. R. MONTIERTH, R. S. GORDON, and I. B. CUTLER, in "Kinetics of Reactions in Ionic Species", edited by T. S. Gray and V. D. Freechette (Plenum Press, New York, 1969) p. 522.
13. A. S. BURTE and P. S. NICHOLSON, *J. Am. Ceram. Soc.* **55** (1972) 469.
14. S. J. KRIDELBAUGH, *Am. J. Soc.* **273** (1973) 757.
15. W. J. THOMSON, in "Ceramic Transactions", Vol. 5, "Advanced Characterization Techniques for Ceramics", edited by W. S. Young, G. L. Mc Vay and G. E. Pike (American Ceramic Society, Westerville, OH, 1989) p. 131.
16. J. P. COUGHLIN and C. J. O'BRIEN, *J. Phys. Chem.* **61** (1951) 767.

17. M. AVRAMI, *J. Chem. Phys.* **7** (1939) 1103.
18. *Idem, ibid.* **8** (1940) 212.
19. *Idem, ibid.* **9** (1941) 177.
20. A. D. ROLLETT, D. J. SROLOVITZ, R. D. DOHERTY and M. P. ANDERSON, *Acta Metall.* **37** (1989) 627.
21. J. D. HANCOCK and J. H. SHARP, *J. Am. Ceram. Soc.* **55** (1972) 74.
22. A. ROSEN, M. S. BURTON and G. V. SMITH, *Trans. Metall. Soc. AIME* **230** (1964) 205.
23. Y. WANG, D. X. LI and W. J. THOMSON, *J. Mater. Res.* **8** (1993) 195.

Received 4 August 1994
and accepted 15 August 1995